Applied Catalysis B: Environmental 92 (2009) 445–453

Contents lists available at ScienceDirect

Applied Catalysis B: Environmental

journal homepage: www.elsevier.com/locate/apcatb

Methyl ethyl ketone combustion over La-transition metal (Cr, Co, Ni, Mn) perovskites

M.C. Álvarez-Galván [a,*], V.A. de la Peña O'Shea [b], G. Arzamendi [c], B. Pawelec [a], L.M. Gandía [c], J.L.G. Fierro [a]

[a] Instituto de Catálisis y Petroleoquímica, CSIC, Cantoblanco, E-28049 Madrid, Spain
[b] Instituto Madrileño de Estudios Avanzados en Energia (IMDEA Energía), C/Tulipán s/n Móstoles, Madrid, Spain
[c] Departamento de Química Aplicada, Edificio de los Acebos, Universidad Pública de Navarra, Campus de Arrosadía s/n, E-31006 Pamplona, Spain

ARTICLE INFO

Article history:
Received 5 June 2009
Received in revised form 23 August 2009
Accepted 5 September 2009
Available online 12 September 2009

Keywords:
Methyl ethyl ketone
Combustion
Perovskite
Potassium doping

ABSTRACT

A series of $LaBO_3$ (B = Cr, Co, Ni, Mn) and $La_{0.9}K_{0.1}MnO_{3+\delta}$ perovskites have been prepared and tested as catalysts in the combustion of methyl ethyl ketone (MEK) at two concentration levels in air. Complete MEK conversion can be achieved for the most concentrated stream (1250 ppmv, WHSV = 425 h^{-1}) at temperatures between 270 °C (manganite) and 345 °C (chromite). Activity is governed by the nature of the cation in position B and related to reducibility, being comparable for manganite activity with that of the much more expensive Pt-supported catalysts. Doping with K of lanthanum manganite produces an increase in surface area, as well as the formation of non-stoichiometric oxygen and a greater proportion of Mn^{4+} on the surface. All these factors may have a role in increasing its activity for catalytic combustion. Catalytic results suggest a marked influence of MEK concentration on the combustion rate. MEK oxidation to CO_2 goes through acetaldehyde as intermediate product; methyl vinyl ketone and diacetyl (2,3-butanedione) were also formed, albeit in very low amounts. Nevertheless, acetaldehyde yield is zero at complete conversion, so the combustion of MEK can be carried out over these perovskite systems with 100% selectivity for CO_2.

1. Introduction

Methyl ethyl ketone (MEK) is a commonly used solvent in chemical industries that is a hazard to human health and the environment, with control required of its emission into the atmosphere by total oxidation. Supported noble metals [1–3], manganese oxide [4], both supported manganese and palladium oxide [5] and perovskite-type oxides [6] have been investigated for the catalytic combustion of MEK. Perovskite-type oxides have long been used as catalysts also for the combustion of methane and for the complete oxidation of other volatile organic compounds (VOCs) [7]. These systems are mixed oxides represented by the general formula ABO_3 where A is usually a lanthanide and B a transition metal. Interest in them lies mainly in their good thermal stability in the high temperature (700–1100 °C) range of operation and in their lower cost than supported noble metals. In some cases, the activity of perovskites in combustion reactions can be comparable to that of noble metal-based catalysts [8]. A wide range of chemical elements can occupy positions A and B in the perovskite structure, and partial substitutions of these cations give rise to multi-component oxides ($A_{1-x}A'_xB_{1-y}B'_yO_3$), in which the mixed or unusual oxidation states of some elements can be stabilized [7]. A relevant feature of perovskites is non-stoichiometry resulting from structural and electronic defects, being better represented by $ABO_{3\pm\delta}$. In this context, the activity of perovskites as oxidation catalysts has been ascribed to several aspects of their surface composition, as well as to their defective nature in relation to the mobility and reactivity of lattice and surface oxygen species [9,10]. Since the synthesis of these bulk materials requires a high temperature that gives low surface area, the main challenge in the development of these systems is to obtain the perovskite structure with high surface area and, hence, improve their catalytic performance [11]. The application of this type of catalysts in reactions that take place at temperatures that are not very high, such as the combustion of VOCs, can be appropriate as it avoids the sintering of the material during reaction.

High activities have been reported in literature with lanthanide perovskites for the combustion of VOCs, such as $La_{0.8}Sr_{0.2}CoO_3$ for the deep oxidation of toluene [12], $LaMnO_3$ for the combustion of acetone, butyl acetate and isopropanol [13] and $LaCoO_3$, $LaMnO_3$,

* Corresponding author at: Instituto de Catálisis y Petroleoquímica, CSIC, c/Marie Curie, 2 Cantoblanco 28049, Madrid, Spain. Tel.: +34 91 5854773; fax: +34 91 5854760.
E-mail address: c.alvarez@icp.csic.es (M.C. Álvarez-Galván).

0926-3373/$ – see front matter © 2009 Elsevier B.V. All rights reserved.
doi:10.1016/j.apcatb.2009.09.006

$La_{0.8}Sr_{0.2}CoO_3$ and $La_{0.8}Sr_{0.2}MnO_3$ for the combustion of toluene and MEK [6]. In this last contribution, Co-containing perovskites were considerably more active than their Mn counterparts.

By partially substituting the A ion with another of lower oxidation state, electroneutrality can be achieved through the formation of oxygen vacancies or the shifting of the B metal toward higher valences. The presence of B^{4+} can increase the activity toward combustion, since the perovskite can act as an oxygen pump toward the molecule that is going to be oxidized, when B^{4+} shifts to B^{3+} [14]. Moreover the partial substitution of A by an ion of lower oxidation state could result in an increase in surface area, as reported in the literature in the case of lanthanum manganite, in which potassium incorporation produces an increase in surface area [15].

In this work, $LaBO_3$ (B = Cr, Co, Ni, Mn) and $La_{0.9}K_{0.1}MnO_{3+\delta}$ perovskites have been prepared and used as catalysts for the oxidation in air of methyl ethyl ketone, a common ambient air pollutant, at two different levels of ketone concentration. Interest has focused on the formation of partially oxidized compounds during the reaction, an aspect that has received little attention [16] in spite of the abundant literature available on VOC combustion. This issue, however, is of great concern since some intermediates are much more harmful than the original pollutant. In the case of lanthanum manganite, potassium incorporation has been considered with the aim of enhancing the catalytic performance of this perovskite system.

2. Experimental

2.1. Catalyst preparation

$LaBO_3$ (B = Cr, Co, Ni, Mn) and $La_{0.9}K_{0.1}MnO_{3+\delta}$ perovskite samples were prepared by amorphous citrate decomposition. A concentrated solution of citric acid was added to a solution of the metal nitrates of appropriate concentration, whereby the ratio of equivalent grams of metal to equivalent grams of citric acid would be unity. The resulting solution was evaporated to dryness at 100 °C. The precursor obtained was then decomposed at 350 °C for 2 h, and finally calcined in air at 700 °C for 4 h. An aliquot of K-substituted sample was also calcined at 900 °C.

2.2. Catalyst characterization

The calcined materials were characterized with Brunauer–Emmett–Teller (BET) specific surface area measurements using nitrogen adsorption at −196 °C, taking a value of 0.162 nm^2 for the cross-section of N_2 molecule adsorbed at this temperature. These measurements were performed with a Micromeritics ASAP 2100 apparatus on samples previously degassed at 150 °C for 12 h.

The oxide catalysts were characterized by powder X-ray diffractometry according to the step-scanning procedure (step size 0.02°; 0.5 s) with a computerized Seifert 3000 diffractometer, using Ni-filtered Cu Kα (λ = 0.15406 nm) radiation and a PW 2200 Bragg–Brentano $\theta/2\theta$ goniometer equipped with a bent graphite monochromator and an automatic slit. The assignment of the various crystalline phases was based on JCPDS powder diffraction file cards. The mean particle size of perovskites was estimated from X-ray line broadening using Scherrer's equation. The lattice parameters and the space group of the samples have been estimated using FullProf Software© (2005 version 2.0) [17].

TPR experiments were conducted on a Micromeritics 2900 device. Prior to reduction, the catalysts (ca. 50 mg) were heated at a rate of 20 °C/min to a final temperature of 300 °C, and kept for 0.5 h at that temperature under a flow of He to remove water and other contaminants. The catalysts were cooled to ambient temperature in the same He flow; then reduced in flowing gas containing 10 vol.% vol. H_2 in Ar at a total flow rate of 50 mL/min, and finally heated at a rate of 15 °C/min to a final temperature of 1000 °C.

Photoelectron spectra (XPS) of the fresh and used catalysts were acquired with a VG Escalab 200R spectrometer equipped with a hemispherical electron analyzer and an Al Kα ($h\nu$ = 1486.6 eV, 1 eV = 1.6302×10^{-19} J) 120 W X-ray source. The powder samples were placed in a pretreatment chamber and degassed at 300 °C. All binding energies (BE) were referred to C 1s line at 284.9 eV.

Elemental chemical analysis was performed to determine the carbon content in the used catalysts. This was accomplished using a Leco CHNS-932 device with an AD-4 PerkinElmer microbalance (resolution 0.1 μg).

2.3. Catalytic performance

The MEK combustion reaction was carried out in a tubular (8 mm i.d.) fixed-bed Pyrex glass reactor at atmospheric pressure. The catalyst (0.1 g), with a particle size in the range of 100–200 μm, was diluted with 0.2 g of inert solids (Pyrex glass beads) with similar particle size, forming a bed of about 20 mm in length. An air stream saturated with MEK (Panreac, PA) was created using a saturator equipped with temperature and pressure control, and then diluted with synthetic air (99.999%), resulting in MEK partial pressures in the reactor feed of 126 or 32 Pa, 1250 or 320 ppmv of MEK, respectively. Prior to each experiment, the catalyst was treated with 100 $cm^3\ min^{-1}$ (STP) of synthetic air for 1 h at 400 °C. In order to evaluate the light-off performance, once the pretreatment of the catalyst is completed, the MEK-air mixture is fed into the reactor while keeping the temperature at 400 °C. The catalytic bed is allowed to stabilize for about 1 h and then the temperature is decreased in order to measure the ignition curves. All the experiments were performed with a total feed flow rate of 550 $cm^3\ min^{-1}$ (STP) and WHSV (feed mass flow rate divided by catalyst weight excluding the inert solids) of 425 h^{-1}. On-line analysis of the product stream was performed on a Hewlett Packard 6890 gas chromatograph, equipped with a HayeSep Q column connected to a TCD for CO_2 determination, and a HP-INNOWax column connected to an FID for MEK and partial oxidation products analysis.

3. Results and discussion

3.1. Characterization results

3.1.1. Textural characterization

Table 1 shows the specific surface area (S_{BET}) data of the prepared samples. As expected for bulk materials, without internal porosity, all the samples have a relatively low S_{BET} (in the range 4.4–14.4 $m^2\ g^{-1}$). The $LaCrO_3$ material records the lowest S_{BET} among all the perovskites studied, and the largest S_{BET} corresponds to the LaKMn-700 sample. While this latter sample records the highest value of BET area (14.4 $m^2\ g^{-1}$), this decreases markedly in its counterpart calcined at 900 °C (9.3 $m^2\ g^{-1}$) due, as will be commented below, to an increase in the average crystallite size. Although parameters such as calcination and type of precursor, among others, determine to a large extent the textural properties of the final material, it can be assumed that obtained surface area values are in the average of those reported in literature for similar perovskites prepared by the citrate method [18–23]. The observed increase in surface area of $LaMnO_3$ with the addition of potassium could be attributed to a decrease in grain size caused by the separation of crystal domains [24], although it cannot be excluded the contribution of segregated species of potassium oxide over the perovskite particles to the observed surface area increase in LaKMn-700 sample.

Table 1
Specific surface area (S_{BET}) and structural characteristics of the perovskite oxides (ABO_3).

Catalyst	Calcination temperature (°C)	Labelling	S_{BET} ($m^2 g^{-1}$)	Space group	Cell parameter			d (nm)[a]
					a	b	c	
$LaCrO_3$	700	LaCr	4.4	*Pnma*	5.477	7.759	5.507	78.5
$LaCoO_3$	700	LaCo	6.5	*R*-3*c*	5.441	5.441	13.118	31.3
$LaNiO_3$	700	LaNi	8.6	*R*-3*m*	5.481	5.481	6.585	16.4
$LaMnO_3$	700	LaMn	5.9	*R*-3*c*	5.513	5.513	13.335	46.4
$La_{0.9}K_{0.1}MnO_3$	700	LaKMn-700	14.4	*R*-3*c*	5.471	5.471	13.366	45.9
$La_{0.9}K_{0.1}MnO_3$	900	LaKMn-900	9.2	*R*-3*c*	5.511	5.511	13.366	117.6

[a] Mean particle size estimated using the Scherrer's equation.

3.1.2. Crystal structure

The X-ray diffraction (XRD) patterns of all samples show sharp and intense peaks corresponding only to crystalline perovskite-like structures (Fig. 1). The lattice parameters obtained for lanthanum chromite $LaCrO_3$ by means of the Rietveld fit agree with those of the orthorhombic structure with space group *Pnma* [25,26]. Powder XRD analysis of $LaCoO_3$ reveals the presence of a pure crystalline perovskite phase with a rhombohedral structure (space group *R*-3*c*) [27]. At the detection limit of the technique (above ca. 3 nm), neither diffraction lines of cobalt oxide nor La_2O_3 phases are detected, which indicates complete incorporation of Co^{3+} and La^{3+} ions into the perovskite $LaCoO_3$ structure. Similarly, the XRD pattern of the $LaNiO_3$ sample belongs to a single-phase perovskite with rhombohedral structure (space group *R*-3*m*) [28]. No diffraction lines are observed for other nickel phases such as La_2NiO_4 and NiO, although they often are in these kinds of samples.

The diffraction pattern of the $LaMnO_3$ sample is closely related to the one that would be expected for a single-phase perovskite structure. The difference between the ideal and observed pattern is the splitting reflections that imply distortions of the lattice from cubic symmetry. These diffraction patterns were refined in the space group *R*-3*c* [29]. Nevertheless, the incorporation of potassium leads to different effects depending on the calcination temperature. For the sample calcined at 700 °C, the incorporation of potassium gives rise to a slight drop in peak intensity. In addition, although the same space group is observed, the XRD profile shows slightly wider peaks than in the K-free counterpart, which makes cell parameter and crystal size calculations difficult. On the other hand, an increase in the cell parameter in c direction and in the crystallite size is observed for the sample calcined at 900 °C.

3.1.3. Redox properties

The temperature-programmed reduction profiles for all the samples are displayed in Fig. 2. All the profiles present two main reduction regions, with the first one being between 180 and 550 °C and the second between 440 and 900 °C. It is also observed that the order of reduction for the $LaBO_3$ (B = Mn, Co, Ni) perovskites is the following: LaNi > LaCo > LaMn. The position of the aforementioned peaks depends on the reduction kinetics, which is influenced mainly by crystallite size and oxygen defects in the perovskite lattice.

Regarding the TPR profile of $LaCrO_3$, a very small peak is observed at around 400 °C (Fig. 2). As reported in the literature

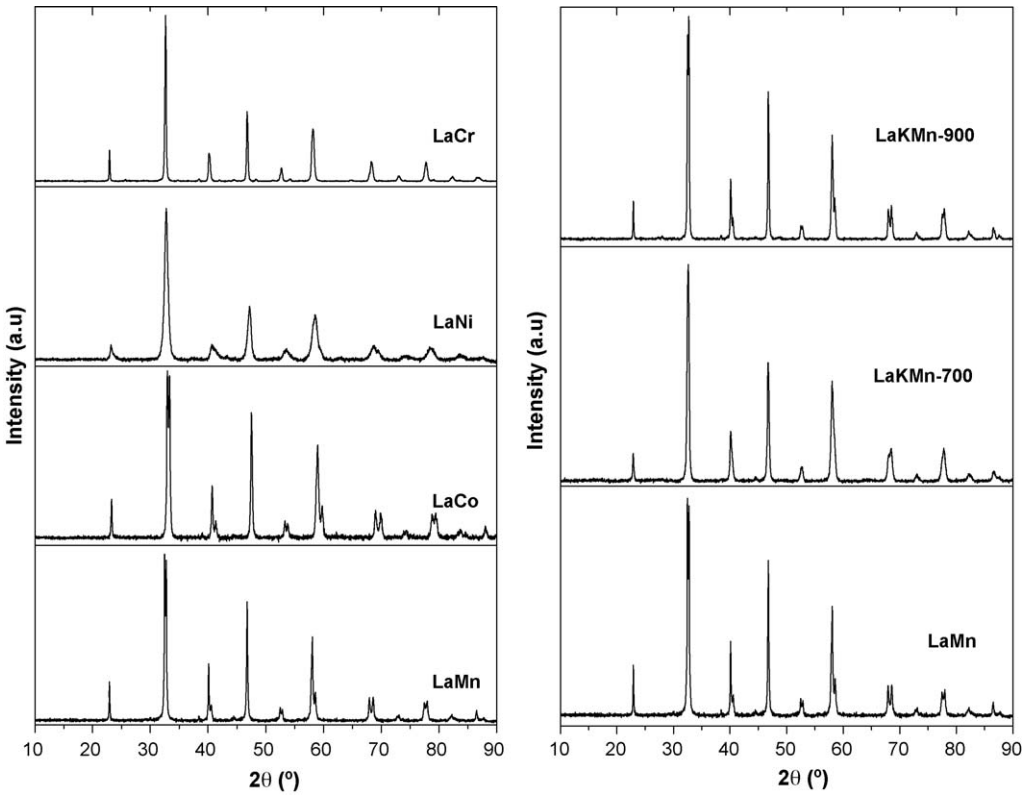

Fig. 1. X-ray diffraction patterns of the calcined perovskite oxides.

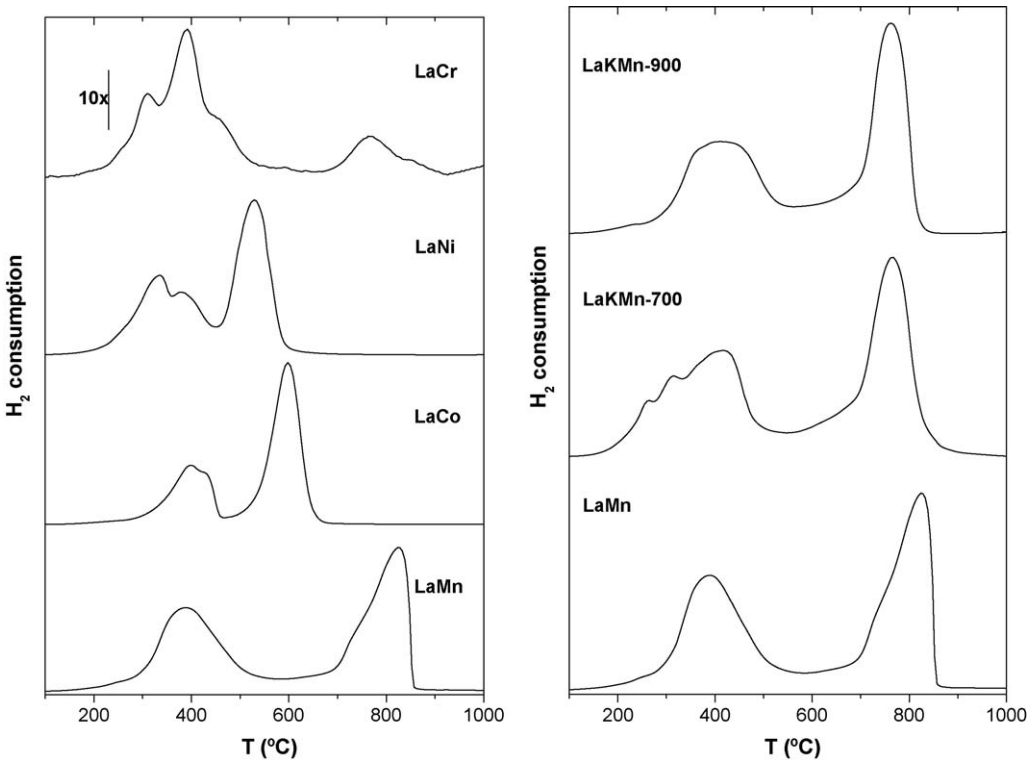

Fig. 2. TPR profiles of the calcined perovskite oxides.

[23], Cr^{3+} ions present in $LaCrO_3$ structure are highly stable and hence cannot be reduced under the experimental conditions employed in this work. The small contribution observed in this profile could be attributed to some La_2CrO_6 formed during the synthesis of the perovskite [30].

In the case of the LaNi sample, the first reduction region is due to a decrease in Ni^{3+} to Ni^{2+} with the concomitant formation of $La_2Ni_2O_5$, while the peak at higher temperature is associated with a reduction of Ni^{2+} ions in the brownmillerite phase to Ni^0 and La_2O_3 [21]. Similarly, the TPR profile of $LaCoO_3$ shows separate peaks that are due to the consecutive reduction of Co^{3+} to Co^{2+} to form $LaCoO_{2.5}$ and to Co^0 dispersed on La_2O_3, respectively [27]. The shoulder observed on the low temperature side of the peak at low temperature for both LaNi and LaCo profiles (Fig. 2) is probably due to the reduction of a small proportion of cobalt or nickel oxide phases as small crystallites not incorporated into the perovskite structure during synthesis.

In the case of the LaMn sample, the hydrogen consumption in the first step is usually assigned to the removal of oxygen from the perovskite structure [31]. The second reduction region is strongly activated and is related to the reduction of Mn(III) to Mn(II), forming MnO, La_2O_3 and small amounts of $La(OH)_3$ [31,32]. Regarding the influence of K incorporation over reducibility, some decrease is observed. The modifications observed in the first region for K-containing samples are associated with the reduction in Mn^{4+} formed to compensate the charge of the K^+ ions incorporated, as well as with some removal of the non-stoichiometric excess of oxygen accommodated within the lattice [32,33].

3.1.4. Surface analysis

The nature of the surface species of all samples was determined by means of X-ray photoelectron spectroscopy. Accordingly, the La 3d, O 1s, Cr 2p, Co 2p, Ni 2p and Mn 2p core-level spectra were recorded and the corresponding binding energies are collected in Table 2.

The La 3d core-level of samples showed the typical profile of lanthanum in $LaBO_3$ compounds [34,35] with the doublets corresponding to spin–orbit ($3d_{5/2}$–$3d_{3/2}$) with peaks at 834.2–834.6 eV and 851.0–851.4 eV, as well as the splitting of each component by ca. 3.5 eV due to the hybridization of 4f orbital phenomena [36] for the $3d^94f^1$ and $3d^94f^0$ final states. Although, the formation of $La_2O_2CO_3$ or $La(OH)_3$ is usual in lanthanum perovskites giving to asymmetry of the La 3d profile, the La 3d profiles have been obtained after a sample pretreatment at 600 °C for 1 h in the pretreatment chamber of the spectrometer to remove most of lanthanum carbonate and hydroxide species. Therefore, the peaks have been adjusted to one component, relative to La in perovskite phase, for all the samples.

The O 1s-core-level spectra of all samples (Fig. 3) showed two different components: the first one at a binding energy of 528.4–529.3 eV, which is characteristic of perovskite lattice oxygen (O^{2-}) [35,37], and a second one at 530.8–531.2 eV, which comes from

Table 2
Binding energies of core-levels of all samples.

	La $3d_{5/2}$	O 1s		Cr 2p		Co 2p	Ni 2p	Mn 2p
$LaCrO_3$	834.2	528.8	530.9	575.6	578.0	–	–	–
$LaCoO_3$	834.2	528.9	531.2	–	–	780.1	–	–
$LaNiO_3$	834.9	528.4	530.9	–	–	–	855.5	–
$LaMnO_3$	834.5	529.0	530.9	–	–	–	–	641.8
$LaKMnO_3$-700	834.6	529.2	530.8	–	–	–	–	642.1
$LaKMnO_3$-900	834.6	529.3	531.0	–	–	–	–	642.0

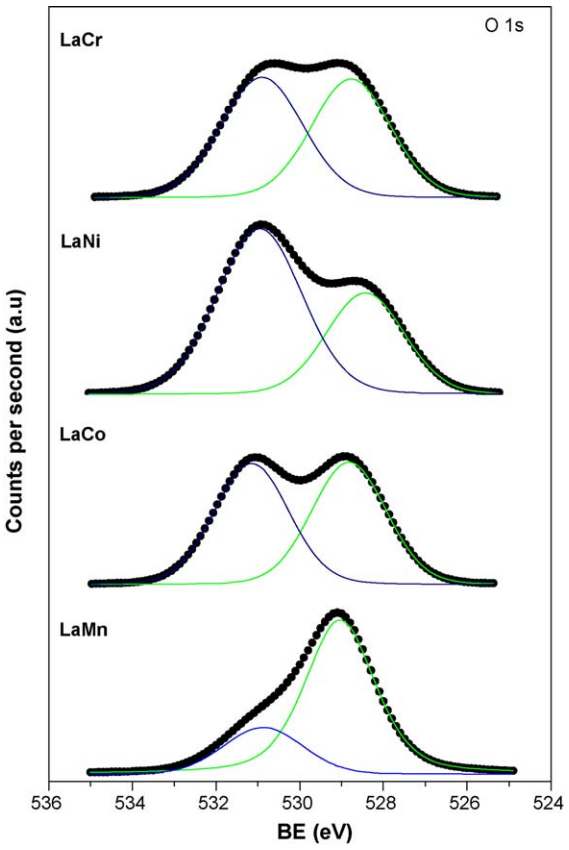

Fig. 3. O 1s-core-level spectra of catalysts.

other O-containing surface species such as carbonate and/or hydroxyl groups [32,38].

The most intense Cr $2p_{3/2}$ component of the Cr 2p doublet of the $LaCrO_3$ sample (Fig. 4) has two peaks at binding energies of 575.6 and 578.0 eV that correspond to Cr^{3+} and Cr^{6+} species, respectively [39,40]. The observation of Cr^{6+} species in $LaCrO_3$ structures is not expected from the stoichiometry of this compound. However, as occurs in chromium oxide (Cr_2O_3), air-calcination at temperatures above ca. 400 °C results in partial oxidation of exposed Cr^{3+} ions into Cr^{6+}. On the other hand, the most intense Co $2p_{3/2}$ component of the Co 2p doublet of $LaCoO_3$ (Fig. 4) appears, as expected for Co^{3+} ions, at a binding energy of 780.1 eV. However, a certain proportion of Co^{2+} ions is also present on the surface of the $LaCoO_3$ material, as can be seen from the observation of a satellite band of the principal Co $2p_{3/2}$ peak, which is the fingerprint of Co^{2+} ions and is, of course, absent in Co^{3+} ions [27,41,42].

The Ni 2p profile in $LaNiO_3$ is complex due to the overlapping of Ni $2p_{3/2}$ and La $3d_{3/2}$ peaks. This overlapping may mask not only the accurate measuring of the BE of nickel but also its intensity. To overcome this complication, the Ni $2p_{3/2}$ + La $3d_{3/2}$ energy region was fitted to four components in decreasing binding energy: shake-up satellite of Ni^{2+}, principal Ni $2p_{3/2}$ and the two split La $3d_{3/2}$ components. The procedure appears to be accurate and the estimated error in triplicate measurements did not exceed ±0.2 eV. The Ni $2p_{3/2}$ binding energy at 855.5 eV reveals the presence of ionic nickel species. Due to the close similarity between the BE of Ni^{2+} and Ni^{3+}, it is difficult, if not impossible, to discriminate between the two species by XP spectra alone. However, the observation of the satellite line, which is the fingerprint of Ni^{2+}, can be taken as conclusive of the presence of an important proportion of Ni^{2+} on the surface.

The chemical state of manganese in $LaMnO_3$ and in K-substituted manganites was also studied by XPS. The binding energies of Mn $2p_{3/2}$ core-levels, compiled in Table 2, are similar for all samples and fall within the range 641.8–642.1 eV. Since the binding energy of Mn^{3+} does not differ substantially from that of Mn^{4+}, the conclusion derived from XPS is that both Mn^{3+} and Mn^{4+} species could coexist on the sample surface. For the K-substituted manganites, one would expect holes to form in the O 2p band. In order to verify the valence state of manganese ions, we used the Galakhov et al. approach [43]. The splitting of the Mn 3s core-level spectrum originates from the exchange coupling between the Mn 3s hole and Mn 3d electrons. The magnitude of this splitting is proportional to (2S + 1), where S is the local spin of the 3d electrons in the ground state [44]. We have firstly recorded the Mn 3s spectra of MnO, Mn_3O_4, Mn_2O_3 and MnO_2 pure oxides and measured their splitting values. In the next step, we have measured the Mn 3s splitting for $LaMnO_3$, $LaKMnO_3$-700 and $LaKMnO_3$-900 catalysts, and the corresponding values are indicated by arrows in Fig. 5. From this plot it is clear that manganese surface species include both oxidation states of +3 and +4. The values obtained for δBE of Mn 3s level correspond to calculated manganese formal oxidation states of +3.46, +3.65 and +4.06 for $LaMnO_3$, $LaKMnO_3$-700 and $LaKMnO_3$-900, respectively. These results indicate that K-substitution by La results in an increase in the proportion of Mn^{4+} on the surface and are consistent with the comment made in the Introduction. On the other hand, the rise in calcination temperature also produces an increase in the oxidation state of Mn.

3.2. Catalytic performance and its relationship with characterization results

The light-off curves for MEK combustion (126 Pa, 1250 ppmv) over the perovskite oxides are shown in Fig. 6. As can be seen, there are significant differences in their catalytic activity. LaKMn-700 was the most active of the perovskites considered, whereas chromite was the least active one. Differences between Co- and Ni-perovskites were not significant and the increase in calcination temperature from 700 to 900 °C has a clear negative effect on the light-off performance of the Mn perovskite. On the basis of the temperature required to achieve 100% MEK conversion, the order of decreasing catalytic activity is as follows: LaKMn-700 (267 °C) > LaKMn-900 ≈ LaMn (297 °C) > LaCo ≈ LaNi (310 °C) > LaCr (345 °C). These results are consistent with the well-known fact that the hydrocarbon oxidation activity of perovskites is governed by the nature of the cation in position B and that the most active catalysts are those containing Mn and Co [7].

The effect of K-loading on the enhancement of catalyst performance results in an increase in specific area and also in the formation of non-stoichiometric oxygen that may have a role in the oxidation reaction. Consideration should also be given to the greater proportion of Mn^{4+} species on the surface that can act as an oxygen pump during the reaction when the ion is reduced to Mn^{3+}. The fact that manganese in the most active sample exhibits a formal oxidation state (+3.65) intermediate between that in LaMn (+3.46) and LaKMn-900 (+4.06) points also to a best balanced Mn^{3+}/Mn^{4+} ratio leading to an improved redox catalytic activity. The action of K increasing the electron donor ability of the catalyst cannot be excluded [45]. Considering the reactivity of the carbonyl group, the increase in the electron density of the catalyst surface should enhance the electrophilic adsorption of ketone molecules, shifting the combustion temperatures towards lower values. This effect was observed when Cs^+ and Na^+ were used as additives for manganese oxide based catalysts in the catalytic combustion of acetone and MEK [4]. Factors such as the loss of surface area for the K-doped sample calcined at higher temperature (LaKMn-900), as well as the large crystallites formed in this system and the absence of non-stoichiometric oxygen (TPR), should

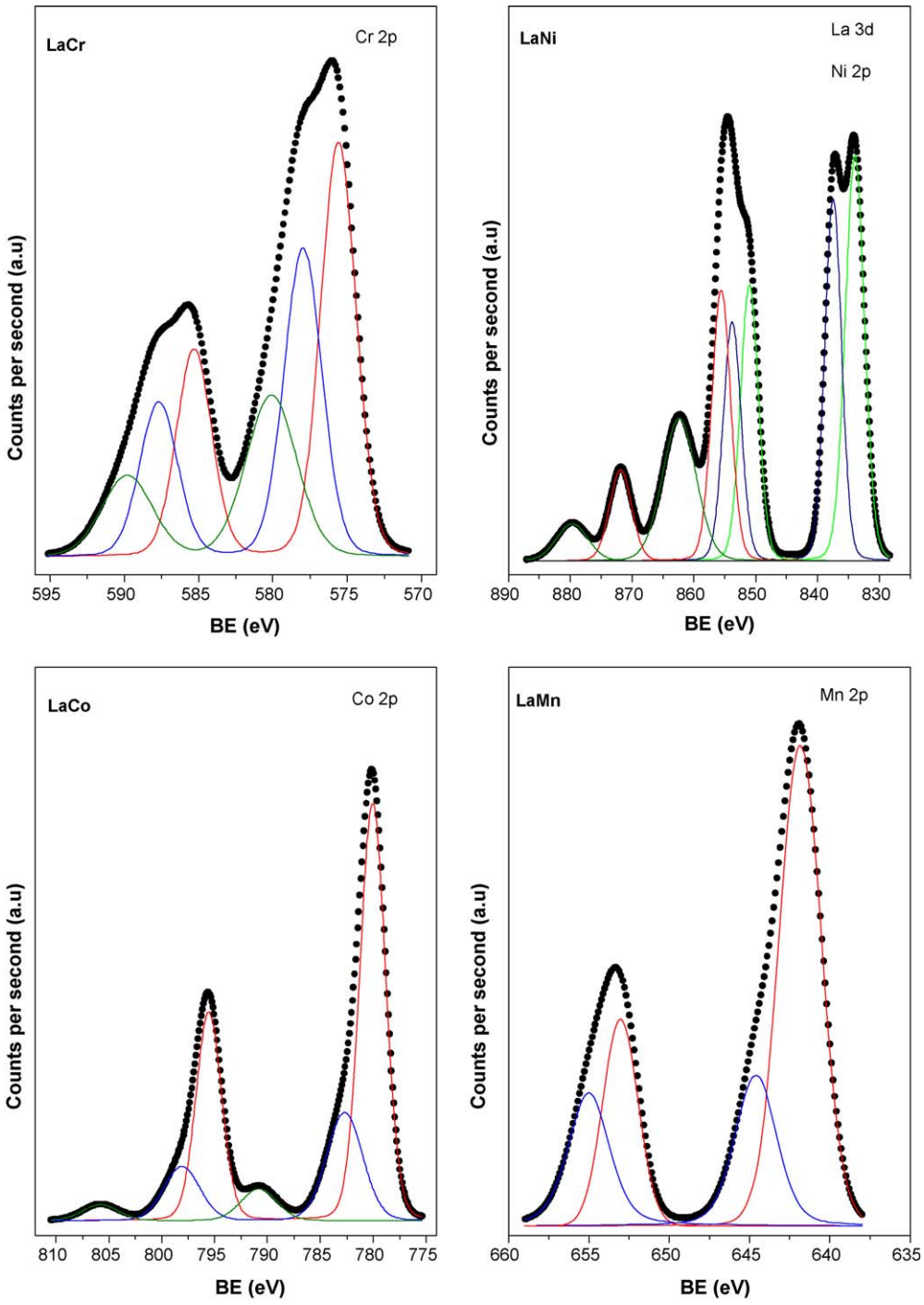

Fig. 4. Cr 2p, Ni 2p, Co 2p and Mn 2p core-level spectra of catalysts.

influence the drop in combustion activity in comparison with its counterpart calcined at 700 °C.

It is known that carbonaceous deposits on the catalysts surface take place during the oxidation of VOCs. Results obtained by elemental chemical analysis indicate that the amount of carbon in used catalysts (Table 3) is influenced by their activity. Thus, the less active catalyst (LaCr) is that with the lowest amount of carbon, and the most active one (LaKMn-700) is the sample that produces more carbon, without considering the contribution coming from adsorbed carbonates.

To the best of our knowledge, the work by Irusta et al. [6] is the only previous report on MEK combustion over perovskites. These authors found complete MEK conversion (162 Pa, WHSV = 178 h^{-1}) at about 280 and 320 °C over Mn and Co lanthanum perovskites, respectively. The fact that the WHSV for the results in Fig. 6 is more than twice the value used by those authors points to a good performance by our perovskite systems. As a matter of fact, the performance of these oxides is not far from that of Pt/alumina catalyst, which allows complete MEK conversion at about 280 °C and WHSV of 734 h^{-1}, as found in our previous study [46].

As concerns the effect of MEK concentration in the feed, the results obtained when decreasing MEK partial pressure from 126 to 32 Pa (1250–320 ppmv) over several perovskites are shown in Fig. 7A and B. The temperature required to reach 100% conversion at constant WHSV decreases as MEK concentration decreases. For this fourfold reduction in MEK concentration, the temperature

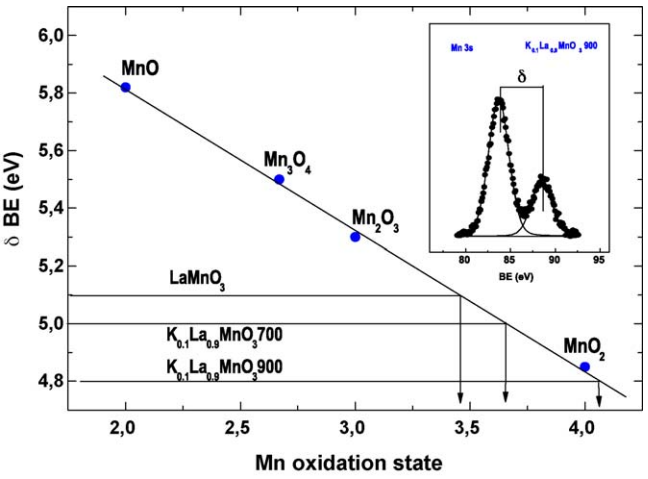

Fig. 5. Dependence of the relative energy between the Mn 3s main peak and its satellite on the formal oxidation state of manganese in pure MnOx oxides and catalysts. The inset Mn 3s spectrum and satellite show how the magnitude of the splitting (δBE) is measured.

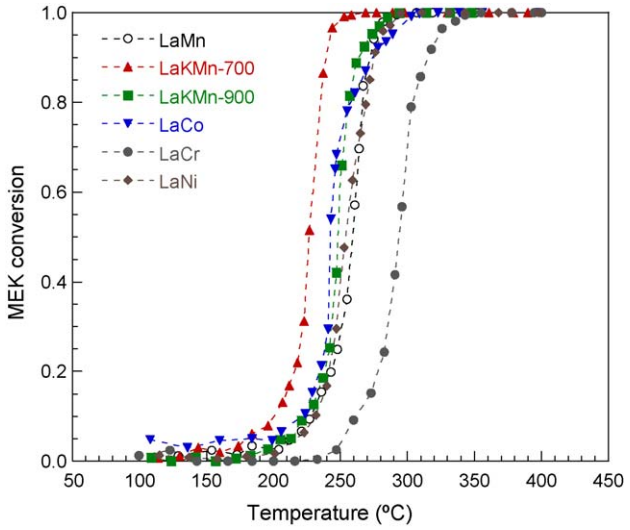

Fig. 6. Light-off curves for MEK (126 Pa) combustion in air over the indicated perovskites; WHSV = 425 h^{-1}.

decreases by about 30 °C for the manganites and by up to 45 °C for the chromite. A remarkable temperature drop of 55 and 60 °C has been measured for the Co- and Ni-perovskites, resulting in values of only 255 and 249 °C, respectively (Fig. 7B). This suggests a marked influence of MEK concentration on the combustion rate that needs further investigation through a specific kinetic study. Irusta et al. found that the apparent reaction order for MEK over the Mn and Co lanthanum perovskites was close to 1 [6].

As regards reaction selectivity, it has been found that MEK oxidation to CO_2 is accompanied by the formation of partially

Table 3
Carbon percentage in used catalysts (elemental chemical analysis).

Catalyst	Calcination temperature (°C)	Labelling	C (wt.%)
$LaCrO_3$	700	LaCr	0.045
$LaCoO_3$	700	LaCo	0.09
$LaNiO_3$	700	LaNi	0.085
$LaMnO_3$	700	LaMn	0.083
$La_{0.9}K_{0.1}MnO_3$	700	LaKMn-700	0.19
$La_{0.9}K_{0.1}MnO_3$	900	LaKMn-900	0.10

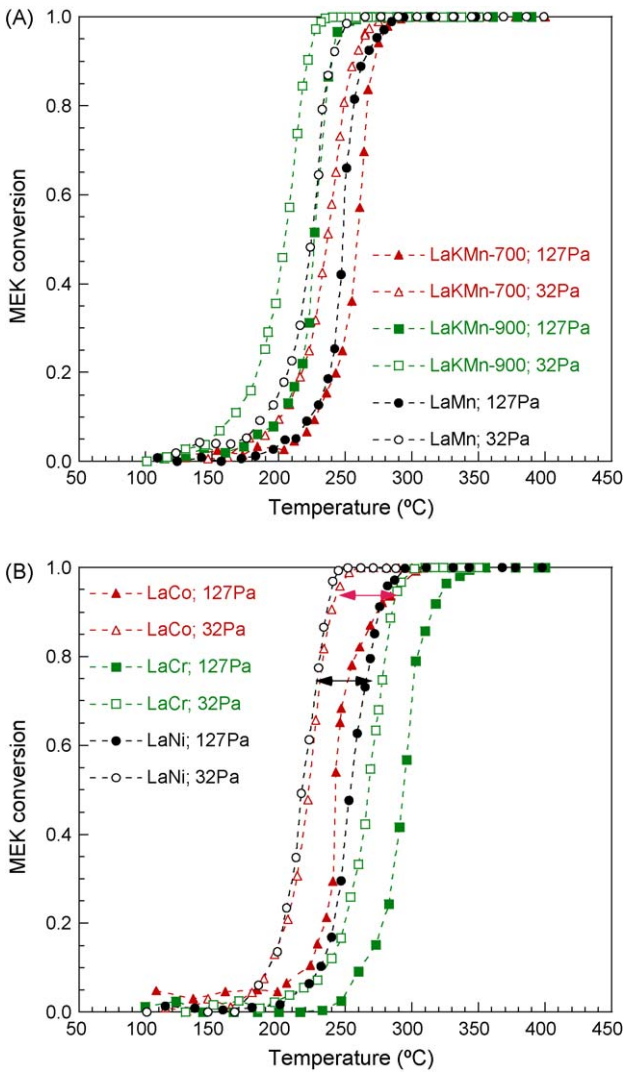

Fig. 7. Light-off curves for MEK (126 and 32 Pa) combustion in air at WHSV = 425 h^{-1} over the perovskites: (A) LaMn, LaKMn-700 and LaKMn-900; (B) LaCo, LaNi and LaCr.

oxidized products, mainly acetaldehyde, but also methyl vinyl ketone (MVK) and diacetyl (2,3-butanedione), although yields for MVK and diacetyl, formed via parallel reactions as proposed by McCullagh et al. [47], were always very low (below 1%). Similar results were found in our previous work on the kinetics of MEK combustion in air over alumina-supported PdOx–MnOx catalysts [5]. The evolution of the acetaldehyde yield as a function of reaction temperature and conversion during the oxidation of MEK (126 Pa, 425 h^{-1}) is shown in Figs. 8 and 9, respectively. Note should first be taken of this lack of selectivity towards MEK complete combustion in contrast with the performance of Pt, since during the combustion of MEK over Pt/alumina the only reaction products found were CO_2 and H_2O [43]. Nevertheless, as shown in Fig. 9, the acetaldehyde yield is zero at complete MEK conversion, that is, the combustion of MEK can be carried out over the perovskites with 100% selectivity for CO_2 at a temperature sufficiently high as to ensure complete conversion. This is a clear advantage considering that these oxides are much cheaper than Pt catalysts. These results clearly indicate that MEK combustion over the perovskites takes place through an acetaldehyde intermediate. The same reaction pathway has been found for the combustion of acetone over $LaMnO_3$ [16]. As can be seen in Fig. 8, the acetaldehyde yield peaks and then decreases to zero as the

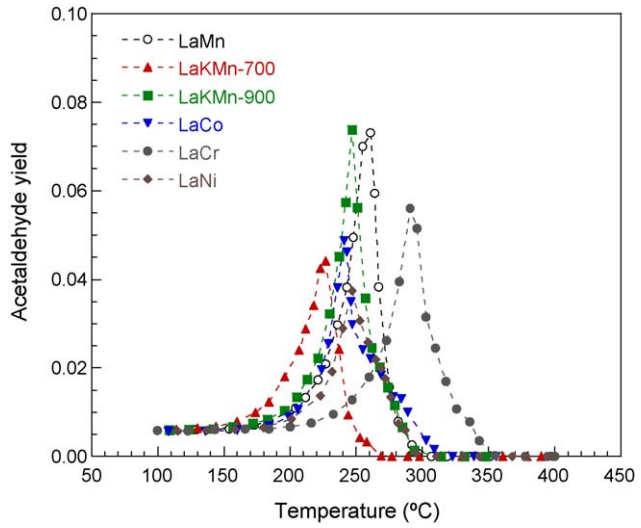

Fig. 8. Acetaldehyde yield vs. MEK combustion temperature.

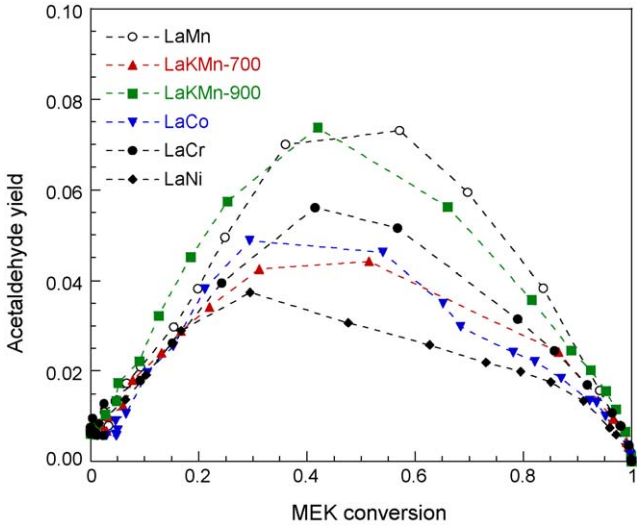

Fig. 9. Acetaldehyde yield vs. MEK conversion.

temperature increases due the combustion of this intermediate to CO_2. Maximum acetaldehyde yields vary between 4% for LaNi and 7.5% for LaKMn-900. Interestingly, the selectivity of the manganite for the partially oxidized products increases with calcination temperature. The maximum yields for acetaldehyde increase slightly as the MEK partial pressure in the feed decreases to 32 Pa: 5% for LaNi and 9% for LaKMn-900.

4. Summary and conclusions

MEK oxidation using $LaBO_3$ (B = Cr, Co, Ni, Mn) and $La_{0.9}K_{0.1}MnO_{3+\delta}$ perovskite catalysts is strongly affected by the element in position B, with a relationship being found between reducibility and activity for the combustion. For 100% MEK conversion, the order of decreasing catalytic activity is as follows: $LaMnO_3 > LaCoO_3 \approx LaNiO_3 > LaCrO_3$.

As concerns the effect of MEK concentration in the feed, the results obtained when decreasing MEK partial pressure from 126 to 32 Pa over three selected perovskites show a substantial decrease in the temperature required to reach 100% conversion at constant WHSV, and this decreases as MEK concentration decreases. This suggests a marked influence of MEK concentration on the combustion rate, even though a specific kinetic study is required to analyze the effect of MEK concentration in detail.

MEK oxidation is accompanied by the formation of partially oxidized products, mainly acetaldehyde, although it should be noted that total oxidation is achieved at complete MEK conversion.

Partial substitution of K by La in $LaMnO_3$ yields the most active catalyst ($La_{0.9}K_{0.1}MnO_3$). Factors such as high surface area, the increase in MEK adsorption capability by increased electron donor ability, and the formation of non-stoichiometric oxygen combined with the greater proportion of Mn^{4+} in the surface are factors that enhance combustion activity. These catalysts have a comparable performance to Pt-supported catalysts, although the perovskite-based systems are much cheaper.

Acknowledgements

G.A. and L.M.G. gratefully acknowledge the financial support provided for this work by the Spanish Ministry of Science and Innovation (MAT2006-12386-C05). Two of us (MCA-G and VAPO) acknowledge financial support from the MCYT in the Ramón y Cajal research programme.

References

[1] J. Hermia, S. Vigneron, Catal. Today 17 (1993) 349.
[2] M.P. Pina, S. Irusta, M. Menendez, J. Santamaria, J.R. Hughes, N. Boag, Ind. Eng. Chem. Res. 36 (1997) 4557.
[3] A. Gil, M.A. Vicente, J.F. Lambert, L.M. Gandía, Catal. Today 68 (2001) 41.
[4] L.M. Gandía, A. Gil, S.A. Korili, Appl. Catal. B: Environ. 33 (2001) 1.
[5] G. Arzamendi, V.A. de la Peña O'Shea, M.C. Álvarez-Galván, J.L.G. Fierro, P.L. Arias, L.M. Gandía, J. Catal. 261 (2009) 50.
[6] S. Irusta, M.P. Pina, M.P. Menendez, J. Santamaria, J. Catal. 179 (1998) 400.
[7] M.A. Peña, J.L.G. Fierro, Chem. Rev. 101 (2001) 1981.
[8] H. Arai, T. Yamada, K. Eguchi, T. Seiyama, Appl. Catal. 26 (1986) 265.
[9] L.G. Tejuca, J.L.G. Fierro, J.M. Tascón, Adv. Catal. 36 (1989) 237.
[10] J.L.G. Fierro, Catal. Today 8 (1990) 153.
[11] K.R. Barnard, K. Foger, T.W. Turney, R.D. Williams, J. Catal. 125 (1990) 265.
[12] C. Chang, H. Weng, Ind. Eng. Chem. Res. 32 (1993) 2930.
[13] H.G. Lintz, K. Wittstock, Catal. Today 29 (1996) 457.
[14] D. Fino, N. Russo, G. Saracco, V. Specchia, J. Catal. 217 (2003) 367.
[15] Y. Ng Lee, R.M. Lago, J.L.G. Fierro, V. Cortés, F. Sapiña, E. Martínez, Appl. Catal. A: Gen. 207 (2001) 17.
[16] A. Musialik-Piotrowska, K. Syczewska, Catal. Today 59 (2000) 269.
[17] J. Rodriguez-Carvajal, Collected Abstracts of Powder Diffraction Meeting, Toulouse, France, 1990, p. 127.
[18] M. Kakihana, M. Arima, M. Yoshimura, N. Ikeda, Y. Sugitani, J. Alloys Compd. 283 (1999) 102.
[19] E. Campagnoli, A. Tavares, L. Fabbrini, I. Rossetti, Y.A. Dubitsky, A. Zaopo, L. Forni, Appl. Catal. B: Environ. 55 (2005) 133.
[20] S. Royer, H. Alamdari, D. Duprez, S. Kaliaguine, Appl. Catal. A: Gen. 282 (2005) 273.
[21] M.E. Rivas, C.E. Hori, J.L.G. Fierro, M.R. Goldwasser, A. Griboval-Constant, J. Power Sources 184 (2008) 265.
[22] G. Carneiro de Araujo, S. Lima, M.C. Rangel, V. La Parola, M.A. Peña, J.L.G. Fierro, Catal. Today 107–108 (2005) 906.
[23] J.L.G. Fierro, L. Gonzalez-Tejuca, J. Catal. 87 (1984) 126.
[24] N. Tien-Thao, M.H. Zahedi-Niaki, H. Alamdari, S. Kaliaguine, J. Catal. 245 (2007) 348.
[25] C.P. Khattak, D.E. Cox, Mater. Res. Bull. 12 (1977) 463.
[26] K. Tezuka, Y. Hinatsu, A. Nakamura, T. Inami, Y. Shimojo, Y. Morii, J. Solid State Chem. 141 (1998) 404.
[27] R.M. Navarro, M.C. Alvarez-Galvan, J.A. Villoria, I.D. Gonzalez-Jimenez, F. Rosa, J.L.G. Fierro, Appl. Catal. B: Environ. 73 (2007) 247.
[28] Z. Zhao, X. Yang, Y. Wu, Appl. Catal. B: Environ. 8 (1996) 281.
[29] R. Doshi, C.B. Alcock, N. Gunasekaan, J.J. Carberry, J. Catal. 140 (1993) 557.
[30] S. Ifrah, A. Kaddouri, P. Gelin, G. Bergeret, Catal. Commun. 8 (2007) 2257.
[31] J.L.G. Fierro, J. Tascon, L. Tejuca, J. Catal. 89 (1984) 209.
[32] S. Ponce, M.A. Peña, J.L.G. Fierro, Appl. Catal. B: Environ. 24 (2000) 193.
[33] E.M. Vogel, D.W. Johnson Jr., P.K. Gallagher, J. Am. Ceram. Soc. 60 (1977) 31.
[34] L. Armelao, D. Barreca, G. Bottaro, A. Gasparotto, C. Maragno, E. Tendello, Surf. Sci. Spectra 10 (2003) 143.
[35] S. Kaliaguine, A. van Neste, V. Szabo, J.E. Gallot, M. Bassir, R. Muzyzchuk, Appl. Catal. A: Gen. 209 (2001) 345.
[36] A.N. Chaika, A.M. Ionov, N.A. Tulina, D.A. Shulyatev, Ya.M. Mukovskii, J. Electron Spectrosc. Relat. Phenom. 148 (2005) 101.
[37] H. Seim, M. Nieminem, L. Niinistö, H. Fjellvåg, L.S. Johansson, Appl. Surf. Sci. 112 (1997) 243.

[38] J.L. Dubois, M. Bisiaux, H. Mimoun, C.J. Cameron, Chem. Lett. (1990) 967.
[39] R. Merryfield, M. McDaniel, G. Munuera, J. Catal. 77 (1982) 348.
[40] B. Wichterlova, L. Krajcikova, Z. Tvaruskova, S. Beran, J. Chem. Soc. Faraday Trans. 80 (1984) 2639.
[41] E. Bontempi, L. Armelao, D. Barreca, L. Bertolo, G. Bottaro, E. Pierangelo, L.E. Depero, Cryst. Eng. 5 (2002) 291.
[42] H.A.E. Hagelin-Weaver, G.B. Hoflund, D. Minahan, G.N. Salaita, Appl. Surf. Sci. 235 (2004) 420.
[43] V.R. Galakhov, M. Demeter, S. Bartkowski, M. Neumann, N.A. Ovechkina, E.Z. Kurmaev, N.I. Labachevskaya, Y.M. Mukoskii, J. Mitchell, D.L. Ederer, Phys. Rev. B 65 (2002) 113102.
[44] I. Barrio, I. Legórburu, M. Montes, M.I. Domínguez, M.A. Centeno, J.A. Odriozola, Catal. Lett. 101 (2005) 151.
[45] V.D. Sokolovskii, Catal. Rev. Sci. Eng. 32 (1990) 1.
[46] G. Arzamendi, R. Ferrero, A.R. Pierna, L.M. Gandía, Ind. Eng. Chem. Res. 46 (2007) 9037.
[47] E. McCullagh, J.B. McMonagle, B.K. Hodnett, Appl. Catal. A 93 (1993) 203.